Since January 2020 Elsevier has created a COVID-19 resource centre with free information in English and Mandarin on the novel coronavirus COVID-19. The COVID-19 resource centre is hosted on Elsevier Connect, the company's public news and information website.

Journal of Drug Delivery Science and Technology 77 (2022) 103921

Contents lists available at ScienceDirect

Journal of Drug Delivery Science and Technology

journal homepage: www.elsevier.com/locate/jddst

Quercitrin loaded cyclodextrin based nanosponge as a promising approach for management of lung cancer and COVID-19

Sally Abou Taleb [a], Yassmin Moatasim [b], Mohamed GabAllah [b], Marwa Hasanein Asfour [a,*]

[a] Pharmaceutical Technology Department, National Research Centre, El-Buhouth Street, Dokki, Cairo, 12622, Egypt
[b] Center of Scientific Excellence for Influenza Viruses, National Research Centre, El-Buhouth Street, Dokki, Cairo, 12622, Egypt

ARTICLE INFO

Keywords:
Quercitrin
Cyclodextrins
Nanosponge
A549 lung cancer cell line
SARS-CoV-2
COVID-19

ABSTRACT

Lung cancer and pandemic acute respiratory disease, COVID-19, are examples of the most worldwide widespread diseases. The aim of the current study is to develop cyclodextrin based nanosponge (CD-NS) for loading the flavonoid drug, quercitrin (QCT). This is to improve its solubility in an attempt to enhance its activity against lung cancer as well as SARS-CoV-2 virus responsible for COVID-19. Preparation of CD-NS was performed by ultrasound-assisted synthesis method. Two CDs were employed, namely, β cyclodextrin (βCD) and 2-hydroxy propyl-β-cyclodextrin (2-HPβCD) that were crosslinked with diphenyl carbonate, one at a time. QCT loaded CD-NS revealed entrapment efficiency and particle size ranged between 94.17 and 99.03% and 97.10–325.90 nm, respectively. QCT loaded 2-HPβCD-NS revealed smaller particle size compared with that of QCT loaded βCD-NS. Zeta potential absolute values of the prepared formulations were >20 mV, indicating physically stable nanosystems. The selected formulations were investigated by Fourier transform infrared spectroscopy, X-ray powder diffraction and scanning electron microscopy which proved the formation of QCT loaded CD-NS exhibiting porous structure. QCT exhibited partial and complete amorphization in βCD-NS and 2-HPβCD-NS, respectively. *In vitro* release revealed an improved release of QCT from CD-NS formulations. The biological activity of free QCT and QCT loaded CD-NS was investigated against lung cancer cell line A549 as well as SARS-CoV-2 virus. The results revealed that IC_{50} values of free QCT against lung cancer cell line A549 and SARS-CoV-2 were higher than those exhibited by QCT loaded CD-NS by 1.57–5.35 and 5.95–26.95 folds, respectively. QCT loaded 2-HPβCD-NS revealed enhanced *in vitro* release and superior biological activity compared with QCT loaded βCD-NS.

1. Introduction

Lung cancer is one of the main common occurring cancers that caused death in 2020 [1]. Most of newly diagnosed patients have locally advanced or metastatic lung cancer that require chemotherapeutic drugs and systemic treatment. Unfortunately, this therapy has limitations due to toxicity and acquisition of drug resistance [2,3]. Recently, effective strategies for prevention of lung cancer have been focused on plant derived dietary supplements which are of low cost, non-toxic and physiologically active [4,5].

Severe Acute Respiratory Syndrome Coronavirus-2 (SARS-CoV-2) is the virus responsible for COVID-19 pandemic acute respiratory disease in 2020; it belongs to the genus Betacoronavirus and subgenus Sarbecovirus. COVID-19 has been first reported from Wuhan, China since December 2019. This pandemic disease has become widespread across the globe, crossing the world countries, that affects a large percentage of the population. Typical clinical symptoms of COVID-19 are headache, dry cough, fever, breathing difficulties and pneumonia. Disease may be progressed into respiratory failure due to alveolar damage and even death [6–8]. Nevertheless, no specific clinical protocol for treatment of COVID-19 has been developed to affect the virus itself. Therapeutic agents of plant derived dietary supplements are preferred due to their safety and low cost.

Flavonoids are a class of low molecular weight polyphenolic biomolecules that are widely present in plants such as vegetables, fruits, flowers, roots and stems. They have gained a huge attention due to attractive biological properties such as anti-oxidant, anti-inflammatory, hepato-protective, anti-cancer, and anti-microbial activities [9,10].

Quercetin derivative (quercetin-3-O-α-L-rhamnoside), known as quercitrin (QCT), is one of the naturally presented glycoside flavonoids;

* Corresponding author.
E-mail address: marwaasfour@hotmail.com (M.H. Asfour).

https://doi.org/10.1016/j.jddst.2022.103921
Received 31 July 2022; Received in revised form 8 October 2022; Accepted 24 October 2022
Available online 28 October 2022

it has a lot of biological activities such as anti-oxidant, anti-bacterial, anti-nociceptive and anti-cancer activity [5,11,12]. Furthermore, ati-viral activity against influenza A virus and corona virus, SARS-CoV-2, has been previously reported for QCT and quercetin based derivatives [13,14].

Many studies have been performed to enhance the aqueous solubility of the hydrophobic drugs in an attempt to enhance their biological activities [15–17]. Unfortunately, QCT is one of the hydrophobic drugs that exhibit limited water solubility (0.064 mg/mL) which hinders its absorption through the biological membranes. Accordingly, for clinical application of QCT, it is necessary to enhance its aqueous solubility as well as its penetration through the biological membranes. Cyclodextrins (CDs) are recognized to be safe pharmaceutical excipients with promising drug delivery potential through fabrication of CD-based delivery systems. CDs are cyclic oligosaccharides with cone-shaped structures exhibiting a hydrophobic cavity, due to the presence of CH_2 groups, and a hydrophilic outer surface due to the presence of primary and secondary OH groups. Thus, they can be complexed with the hydrophobic drug moiety bound to the inner hydrophobic cavity, while the hydrophilic outer surface helps in drug solubilization. There are three natural CDs, namely, alpha-cyclodextrin (αCD), beta-cyclodextrin (βCD), and gamma-cyclodextrin (γCD) with 6, 7, and 8 glucopyranose units, respectively [17–19].

Recently, CDs-based nanosponges (CD-NS) have gained a great attention due to their superior characteristics. CD-NS are innovative crosslinked CDs exhibiting nanostructured network of three-dimensions. They are very porous colloidal carriers that preserve the characteristic properties of CDs such as altering drug solubility, improving drug bioavailability, being nontoxic and biodegradable [20,21]. Interestingly, CD-NS offers improved properties over CDs such as modulation of drug release by controlling crosslinking degree and enhancing inclusion capacities [20,22]. CD-NS can encapsulate poorly water soluble drugs to their inner nanocavities similar to CDs. In addition to their inner nanocavities, that can form inclusion complex with the drug, the external networks formed after crosslinking form tiny mesh-like structures that serve as sites for drug loading by forming non-inclusion complexes [17,23,24]. An early report postulated that dexamethasone was entrapped within NS colloidal matrix, in addition to βCD cavities, that enhanced dexamethasone solubility and loading [25]. Accordingly, CD-NS provides higher sites for interaction, thus higher drug encapsulation compared with plain CD. Therefore, CD-NS attains higher efficiency of drug solubilization compared with CDs [22,25]. Ultrasound irradiation have been profusely employed for successful preparation of CD-NS as early reported [25].

CD-NS has been recently investigated for their potential in drug delivery. For instance, they have been reported to improve stability [24], anti-cancer [26–28], anti-inflammatory [29] and anti-viral activity of the active agents [30,31].

Regarding the abovementioned premises, the aim of the current study is to fabricate a nano-carrier system, CD-NS, loaded with QCT to improve its solubility in an attempt to enhance its anti-proliferative and anti-SARS-CoV-2 activities. The current research work comprised preparation and *in vitro* investigation of two different CD-NS systems loaded with QCT. The successfully developed QCT loaded CD-NS formulations were investigated for their anti-proliferative activity employing lung cancer cell line A549. Moreover, anti-SARS-CoV-2 activity employing Egyptian SARS-CoV-2 was investigated to the developed formulations. To the best of our knowledge, drugs which reveal activity against SARS-CoV-2 have not been widely investigated as a part of drug delivery nanosystem [32]. This article investigated the potential of drug delivery nanosystems to combat COVID-19.

2. Materials and methods

2.1. Materials

Quercitrin (QCT) was kindly obtained as a gift sample, by Aljubiri et al., extracted and highly purified from Saudi Arabia plant (*Euphorbia schimperiana*) as previously reported [33]. 2-hydroxy propyl-β-cyclodextrin (2-HPβCD) was bought from Cyclolab, Hungary. Diphenyl carbonate (DPC) and β-cyclodextrin (βCD) were purchased from Acros Organics, Belgium. All other chemical reagents were of analytical grade.

Human lung cancer A549 and normal Vero-E6 cell lines were purchased from ATCC (American Type Culture Collection, CCL-75™). Roswell Park Memorial Institute (RPMI) media and (3-(4,5-Dimethylthiazol-2-yl)-2,5-diphenyltetrazolium bromide (MTT) were purchased from Bio Basic Inc, Canada. SARS-CoV-2 virus (hCoV-19/Egypt/NRC-03/2020) was isolated and sequenced at the center of scientific excellence for influenza viruses (CSEIV) at the National Research Centre NRC-Egypt [34].

2.2. Methods

2.2.1. Preparation of plain CD-NS

Plain CD-NS were prepared via ultrasound-assisted synthesis method [35–37]. DPC was used as a crosslinker for two types of CDs, namely, βCD and 2-HPβCD. Two molar ratios were employed between each type of CDs and DPC, viz., 1:3 and 1:6, thus four CD-NS formulations were developed (Table 1). Briefly, each type of CD, one at a time, and DPC were mixed in a conical flask. The mixture was gradually heated (90–100 °C) in an ultrasonic water bath sonicator (Elmasonic S 40H, Elma Schmidbauer GmbH, Germany) and allowed to react for 5 h. The mixture of reaction was cooled and then phenol crystals, appeared at the neck of the flask, were carefully removed. The resulted solid product was broken up and then repeatedly washed with distilled water to get rid of unreacted CDs and then with absolute ethanol to remove the unreacted DPC as well as the phenol produced as a reaction by-product. Test for phenol was performed, after every washing, by adding 2 drops of ferric chloride solution (1%w/v) to the washing water [37]. The resulted plain CD-NS was a fine white powder, dried at 40 °C, and stored in a desiccator at room temperature till further use. The yield % for plain CD-NS was calculated using the following equation [37]:

$$\text{Yield}\% = \frac{\text{Weight of CD} - \text{NS}}{\text{Weight of CD} + \text{Weight of DPC}} \times 100$$

2.2.2. Preparation of QCT loaded CD-NS

QCT loaded CD-NS were prepared employing freeze-drying technique as previously reported [36,38]. Accurately weighed quantities of plain CD-NS (200 mg) were dispersed in 20 ml distilled water followed by homogenization employing high speed homogenizer (Heidolph, SilentCrusher M, Germany) at 20,000 rpm for 10 min to reduce the particle size [27]. Thereafter, calculated amount of QCT was added to

Table (1)
Composition and yield (%) of cyclodextrin based nanosponge (CD-NS) employing diphenyl carbonate (DPC) as a crosslinker (n = 3).

Plain CD-NS formula code	CD type	CD:DPC molar ratio	Amount of CD (g)	Amount of DPC (g)	Yield (%) ± SD
BCD/DPC 1:3	βCD	1:3	2.27	1.29	40.32 ± 2.05
BCD/DPC 1:6	βCD	1:6	2.27	2.57	44.17 ± 1.67
HPBCD/DPC 1:3	2-HPβCD	1:3	2.76	1.29	42.76 ± 2.45
HPBCD/DPC 1:6	2-HPβCD	1:6	2.76	2.57	46.01 ± 3.02

the above dispersion in a w/w ratio of 4:1 (CD-NS:QCT); the mixture was sonicated for 20 min. Samples were then incubated in the dark at room temperature under stirring for 24 h to promote the loading of QCT [27]. The obtained suspensions were centrifuged at 2000 rpm (Hanil Co., Union 32R, Korea) for 30 min to separate the un-entrapped QCT as a residue below the colloidal supernatant which is then filtered through a 0.45 μm filter. The filtrate was lyophilized at −60 °C, under pressure of 0.001 bar for 24 h employing Freeze dryer (Alpha 1–4 LSCplus, Germany) to obtain fluffy powder of QCT loaded CD-NS.

2.2.3. Estimation of entrapment efficiency and drug loading for QCT

Accurately weighed amounts of QCT loaded CD-NS systems were dispersed in methanol followed by sonication for about 10 min in order to break the nanosystems [23,36,39]. The prepared samples were analyzed using the UV–Vis recording spectrophotometer (UV-2401 PC, Shimadzu Co., Japan) at 256 nm after appropriate dilution with methanol. The amount of QCT in methanolic solutions of the prepared samples denoted the weight of QCT in CD-NS. The analysis was done in triplicate; entrapment efficiency (EE%) and drug loading (DL%) for QCT were calculated using the following equations [36]:

$$EE\% = \frac{\text{Weight of QCT in CD} - \text{NS}}{\text{Weight of initially added QCT}} \times 100$$

$$DL\% = \frac{\text{Weight of QCT in CD} - \text{NS}}{\text{Total weight of CD} - \text{NS}} \times 100$$

2.2.4. Characterization of QCT loaded CD-NS

2.2.4.1. Determination of particle size, polydispersity index and zeta potential. Particle size (PS), polydispersity index (PDI) and zeta potential (ZP) of QCT loaded CD-NS were estimated by dynamic light scattering (DLS) employing Zeta-sizer (Nano Series ZS90, Malvern Instruments Ltd., Worcestershire, UK). QCT loaded CD-NS were dispersed in double distilled water. The mean value of the measurement was calculated from three independent samples.

2.2.4.2. Scanning electron microscopy. Surfaces of the selected QCT loaded CD-NS were examined with scanning electron microscopy (SEM) (Quanta FEG 250, ThermoFisher Scientific Co., Czech Republic). Freeze dried samples were fixed on aluminum stubs with double-sided tape, coated with a thin gold layer using a sputter coater unit. SEM was operated at an acceleration voltage of 20 kV and a distance of 10 mm.

2.2.4.3. Fourier transform infrared spectroscopy analysis. The possible interaction between QCT and components of the selected CD-NS formulations was detected with fourier transform infrared spectroscopy (FT-IR) analysis, employing KBr pellet method, using FT-IR spectrophotometer (JASCO 6100, Tokyo, Japan).

2.2.4.4. X-ray powder diffraction. Samples were evaluated employing X-ray powder diffraction (XRPD) in order to investigate the effect of CD-NS formulations on crystallinity of QCT. Diffraction patterns were obtained utilizing the X-ray powder diffractometer (Malvern Panalytical Ltd., Empyrean, UK). The X-ray generator was operated at 30 mA tube current and 45 kV tube voltages, using the Kα lines of copper as the radiation source. The diffraction angle ranged between 4 and 75° of (2θ) range in the step scan mode with a step size of 0.026° 2θ and a step time of 21.42 s.

2.2.4.5. Differential scanning calorimetry. Differential scanning calorimetry (DSC) was also performed to investigate the physical state of QCT in the selected CD-NS formulations, using differential scanning calorimeter (Setaram Inc., DSC131 evo, France). Nitrogen and helium were employed as the purging gases. Samples were put in an aluminum pan that is placed in the DSC apparatus and scanned over a temperature ranged between 25 and 350 °C at a rate of 10 °C/min. Thermograms were processed employing Calisto data processing software v.149.

2.2.5. In vitro release profile of QCT from the prepared CD-NS formulations

In vitro release profile of QCT was investigated for the selected formulations and the free QCT suspension using dialysis bag diffusion technique [15,40]. CD-NS formulations as well as free QCT were dispersed in distilled water. Based on calculated DL%, amount equivalent to 1 mg QCT of each sample was dispersed in one ml distilled water and then added into a presoaked cellulose dialysis bag (Dialysis tubing cellulose membrane, Sigma Co., USA; Molecular weight cutoff 12, 000–14,000) that is closed at both ends. Thereafter, the bags were inserted in tightly closed glass bottles containing 50 ml of the release medium, namely phosphate-buffered saline (PBS) pH 7.4, a physiological pH, comprising 15% (v/v) methanol to achieve sink condition for QCT. The bottles were maintained at 37 °C ± 0.50 °C with a rotating speed of 50 rpm, utilizing a thermo-stated shaking water bath (Memmert, SV 1422, Germany). At several time intervals, 1 ml of the release medium were withdrawn and replenished with the same volume of fresh medium to maintain the sink condition. Amount of QCT in each sample was analyzed at 268.6 nm by spectrophotometric assay. At each time interval, the cumulative percentages of QCT released were calculated as the ratio of the released QCT amount to the initial amount of QCT in the dialysis bag. The results were represented as the mean of 3 values ± SD. The release efficiency ($RE_{(0-24hr)}$ %) was assessed by calculating the area under the cumulative percentages of QCT released versus time curve using the trapezoidal rule. The calculated area was expressed as a percentage of the rectangle area that corresponds 100% release, for the total time of the release experiment (24 h), applying the following equation [41]:

$$RE = \left(\frac{\int_0^t y.dt}{y_{100}.t} \right) \times 100$$

Where, y is the cumulative drug released percentage as a function of time and y_{100} is 100% drug released.

Kinetic analysis was carried out for the data of *in vitro* QCT release to assess the release mechanism. The data were fitted with different kinetic equations, viz., zero order (% cumulative drug released vs. time), first order (log% cumulative drug remained vs. time) and Higuchi (% cumulative drug released vs. square root of time) [42]. The proper release model was assessed according to the regression coefficient (R^2) obtained from linear regression analysis for the release data. Release model revealing R^2 value close to one was supposed as the best fit model.

2.2.6. In vitro anti-proliferative activity

This evaluation was carried out by comparing the anti-proliferative activity of free QCT, QCT-loaded CD-NS, and plain CD-NS on human lung cancer cell line A549.

2.2.6.1. Cell culture. 96 well tissue culture plates were inoculated with 1×10^5 cells/ml (100 μl/well) along with the growth medium (RPMI); and then incubated for 24 h at 37 °C to form a complete monolayer sheet. Thereafter, growth medium was decanted from 96 well micro titer plates after confluent sheet of cells were developed, cell monolayer was washed two times with PBS.

2.2.6.2. MTT assay of anti-proliferative activity. Potential anti-proliferative activity of different samples was tested employing MTT assay [43]. Dilutions of tested samples were made in RPMI medium containing 2% serum (maintenance medium). For free QCT and QCT loaded CD-NS, concentrations of 31.25, 62.50, 125, 250, 500 and 1000 μg/ml were used. The same was performed for the plain CD-NS for comparative evaluation. For QCT loaded CD-NS, the equivalent concentration of QCT in each dilution was estimated based on the calculated

DL%. 0.1 ml of each dilution was tested in different wells leaving 3 wells as control that received only maintenance medium. Afterwards, plate was incubated for 72 h at 37 °C, then 20 μl MTT solution (5 mg/ml in PBS) was added to each well. MTT is a yellow compound that is reduced to dark purple formazan by the viable cells. Plates were shaken at 150 rpm for 5 min for complete mixing of MTT into the media. Thereafter, plates were incubated at 37 °C with 5% CO_2 for 1–5 h to allow metabolization of MTT. The metabolic product of MTT, formazan, was re-suspended in 200 μl DMSO and allowed to be shaken, in the dark, at 150 rpm for 30 min to ensure dissolving of formazan in DMSO [44]. Optical densities were read at 560 nm employing a multiwall microplate reader (Synergy HT, Biotech, France), and subtract background at 620 nm. Optical density (OD) should be directly correlated with cell quantity. For each concentration, triplicate wells were prepared. Cell viability and anti-proliferative activity % were calculated in addition to the half maximal inhibitory concentration, IC_{50}, for each sample. Cell viability was determined as a percentage of the viable treated cells in comparison with the number of viable untreated control cells according to the formula [15]:

$$\text{Viability } (\%) = \frac{\text{Optical density (treated cells)}}{\text{Optical density (control cells)}} \times 100$$

Anti-proliferative activity % (inhibition percentage of cell viability) = 100-viability %

2.2.7. Anti-SARS-CoV-2 activity

This evaluation took place by comparing anti-SARS-CoV-2 activity of free QCT, QCT loaded CD-NS, and plain CD-NS against Egyptian SARS-CoV-2 (hCoV-19/Egypt/NRC-03/2020) [34]. Cytotoxicity on normal Vero-E6 cells was also investigated to ensure the safety of the tested samples.

2.2.7.1. Viral titration. Virus isolate was first titrated using VERO-E6 cells subcultured and seeded in 96 well plates to form a mono layer. The culture medium is Dulbecco's Modified Eagle's medium (DMEM) supplemented with 10% Fetal Bovine Serum and 1% Penicillin/Streptomycin antibiotic mixture at 37 °C, 5% CO_2. After 24 h, confluent cell monolayers were treated with a serial dilution of the virus and incubated at 37 °C in 5% CO_2 incubator for 72 h post infection. The plate was then fixed with 100 μL of 4% paraformaldehyde for 90 min and then stained with 0.1% crystal violet in distilled water for 15 min at room temperature. Excess stain was then washed with water and the residual stain was then dissolved with 100 μL absolute methanol per well. The color intensity was measured at 570 nm using Anthos Zenyth 200rt plate reader (Anthos Labtec Instruments, Heerhugowaard, Netherlands) [45,46]. Median tissue culture infectious dose ($TCID_{50}$) was then calculated as the dose or concentration of the virus required to kill 50% of the cells.

2.2.7.2. Determination of cytotoxic concentration 50 (CC_{50}) for normal Vero-E6 cells and inhibitory concentration 50 (IC_{50}) for SARS-CoV-2. The titrated virus was used as 100 $TCID_{50}$ dilution to determine the concentration of the tested samples required to inhibit viral replication. First, serial dilutions of each sample (free QCT, QCT-loaded CD-NS, and plain CD-NS) were used to treat monolayers of Vero-E6 in 96 well plates, in triplicate. Another 96 well plates were inoculated with serial dilutions of the samples that are incubated for 60 min with the 100 $TCID_{50}$ dilution of the virus and then used to treat monolayers of VERO-E6 cells, in triplicate. After incubation for 72 h, cells were fixed and stained as previously described. Untreated and virus infected VERO-E6 cells were used as cell and virus control, respectively.

The wells of cells treated with serially diluted samples without the virus were used to determine the half maximal cytotoxic concentration of each treatment (CC_{50}) which is the concentration responsible for the death of 50% of the cell's monolayers relative to cell control. While the wells of cells inoculated with serially diluted samples treated with the SARS-CoV-2 virus were used to determine the half-maximal inhibitory concentration (IC_{50}) that is required to inhibit the viral propagation by 50% relative to the virus control. For QCT loaded CD-NS, the equivalent concentration of QCT in each dilution was estimated based on the calculated DL%. Selectivity index (SI), which is the ratio between CC_{50} and IC_{50} of the tested sample, was also calculated [47]. From the observed biological properties, the CC_{50} and IC_{50} curves were obtained using GraphPad Prism (version 5.01); data values were transformed, normalized and expressed as the best-fit value.

2.2.8. Statistical analysis

Results were expressed as mean ± standard deviation (SD). Comparisons between different groups were assessed using one-way analysis of variance (ANOVA) followed by Fisher's LSD post-hoc test for multiple comparisons using SPSS software (version 22.0; IBM Co., USA). The difference was considered significant at $p < 0.05$.

3. Results and discussion

3.1. Preparation of plain and QCT loaded CD-NS

Yield % values of plain CD-NS formulations employing CD:DPC molar ratio 1:6 were slightly higher than their counterparts employing CD:DPC molar ratio 1:3 (Table 1). This could be attributed to the high concentration of the crosslinker (DPC) which tends to form additional networks of CD-NS [37].

Regarding QCT loaded CD-NS formulations; fluffy powders were obtained for the developed CD-NS formulations prepared from two types of CDs, namely, βCD or 2-HPβCD crosslinked with DPC, using a w/w ratio of 4:1 between CD-NS and QCT. The employed ultrasound-assisted synthesis method is devoid of the use of organic solvent providing a safe drug delivery system.

3.2. Estimation of entrapment efficiency and drug loading for QCT

Table (2) reveals EE% and DL% for the developed QCT loaded CD-NS formulations. The high EE% could be ascribed to the complete entrapment of the guest drug molecules, as an inclusion complex, into the hydrophobic host cyclodextrins' cavities surrounded by hydrophilic nano-channels in addition to encasement of QCT in the porous matrix of nanosponge [36,48].

3.3. Characterization of QCT loaded CD-NS

3.3.1. Determination of particle size, polydispersity index and zeta potential

The prepared QCT loaded CD-NS formulations revealed PS in nanosize range (Table 2). It is observed that formulations comprising higher molar ratio of crosslinker exhibited PS larger than those comprising lower molar ratio of crosslinker, for the two types of employed CD. This finding is in a good agreement with a previous report [23], where the increase of crosslinker molar ratio resulted in larger PS.

Table (2)
Entrapment efficiency (EE%), drug loading (DL%), particle size (PS), polydispersity index (PDI) and zeta potential (ZP) of QCT loaded cyclodextrin based nanosponge formulations (CD-NS) (n = 3).

QCT loaded CD-NS formula code	EE (%) ± SD	DL (%) ± SD	PS (nm) ± SD	PDI	ZP (mV) ± SD
QCT-BCD/DPC 1:3	95.13 ± 4.53	19.21 ± 0.75	249 ± 15.63	0.31	−21.60 ± 1.70
QCT-BCD/DPC 1:6	94.17 ± 6.16	19.06 ± 1.26	325.9 ± 26.71	0.34	−24.00 ± 2.01
QCT-HPBCD/DPC 1:3	99.03 ± 5.64	19.84 ± 0.98	97.1 ± 8.05	0.25	−24.80 ± 1.15
QCT-HPBCD/DPC 1:6	98.95 ± 7.81	19.83 ± 1.45	280.1 ± 22.67	0.26	−23.50 ± 0.87

PDI for all the investigated nanosponge formulations was <0.4, which is consistent with previous reports [36,49]; this indicates homogenous size distribution of the dispersed particles [15,50]. Table 2 also reveals that all the investigated formulations exhibited a negatively charged zeta potential; this could be due to carbonyl groups of DPC and the free hydroxyl groups of βCD and 2-HPβCD [37,51]. The absolute ZP values for all investigated formulations was higher than 20; these values are quite sufficient for the individual particles to be kept separated from each other due to electric repulsion [15,51]. Thus, the dispersed particles are physically stable. According to results of PS, QCT loaded CD-NS formulations, viz., QCT-BCD/DPC 1:3 and QCT-HPBCD/DPC 1:3 were selected for further investigations.

3.3.2. Scanning electron microscopy

SEM (Fig. 1) reveals the characteristic sponge-like morphology of QCT loaded CD-NS. Samples exhibited a highly porous nature; this is favorable for increased loading of the drug [23].

3.3.3. Fourier transform infrared spectroscopy analysis

Chemical structure of QCT, βCD, 2-HPβCD and DPC are depicted in Fig. 2.

FT-IR spectra of free QCT, CDs (βCD and 2-HPβCD), two types of QCT-loaded CD-NS (QCT-BCD/DPC 1:3 and QCT-HPBCD/DPC1:3) and their corresponding plain CD-NSs are shown in Fig. 3. FT-IR absorption frequencies of peaks of interest are summarized in Table 3.

FT-IR spectra of the two types of plain CD-NSs were almost similar to CD spectra; the difference was only in the presence of peak at about 1770 cm^{-1} of carbonate ester group (pointed by dotted arrows). This indicates that carbonate linkage was added to the primary OH groups of the pure CD and confirming the formation of carbonate based CD-NS. This peak was absent in the FTIR spectra of pure CD. This data is consistent with that previously reported for CD-NS [24,36,52].

FT-IR spectra of the two types of QCT loaded CD-NS (QCT-BCD/DPC 1:3 and QCT-HPBCD/DPC 1:3) exhibited an apparent change in finger print region (400-1400 cm^{-1}) compared with QCT spectrum. Furthermore, the peaks related to O–H stretching of plain CD-NS were shifted to lower wave numbers for the two types of QCT loaded CD-NS (Fig. 3) signifying interaction of OH groups of NS with QCT. This data indicates complexation of QCT within CD-NS; similar findings have been previously reported [37–39]. Unlike plain CD-NS, C=C stretching vibration peak of QCT appeared in FT-IR spectra of the two types of QCT loaded CD-NS as depicted in Table 3 and Fig. 3. Similarly, C=O stretching vibration peak of QCT appeared in FT-IR spectra of the two types of QCT loaded CD-NS (Table 3 and Fig. 3). This is a further confirmation for complexation of QCT with CD-NS.

3.3.4. X-ray powder diffraction

Free QCT, CDs (βCD and 2-HPβCD), two types of QCT-loaded CD-NS (QCT-BCD/DPC 1:3 and QCT-HPBCD/DPC 1:3) and their corresponding plain CD-NSs were evaluated by XRPD analysis to assess their crystallinity. As shown in Fig. 4, X-ray diffractogram of QCT revealed several sharp peaks at 2θ of 6.87, 13.26, 15.20, 17.19, 18.02, 20.32 and 26.45° demonstrating the high crystalline nature of QCT. Similarly, both DPC and βCD diffractograms indicated their crystalline nature, while 2-HPβCD was amorphous where it revealed two broad peaks ranged between 10–15° and 15–20°; these findings are consistent with that previously reported [53,54]. Regarding QCT-BCD/DPC 1:3, the diffractogram indicated a marked reduction in the crystalline peaks' intensities of QCT revealing that QCT lost most of its crystallinity inside CD-NS pores; this indicates its almost amorphous nature. This could be ascribed to formation of inclusion and non-inclusion complexes of the drug with CD-NS [39,55]. Diffractogram of QCT-HPBCD/DPC 1:3 revealed a complete absence of the sharp QCT peaks; this clearly reveals that QCT is encapsulated in a complete amorphous form. Diffractograms of the plain CD-NS and QCT loaded CD-NS were quite different, this could be explained by reorientation of QCT in the polymeric network of CD-NS; similar finding has been reported [55]. It is worthy to note that, unlike the diffractograms of plain and QCT-BCD/DPC 1:3; diffractogram of plain and QCT-HPBCD/DPC 1:3 exhibited complete disappearance of crystalline peaks of DPC and QCT.

In fact, the freeze drying process could provide fluffy mass amorphous powder exhibiting highly porous structure [39]. The free energy of amorphous solid state is much more than its crystalline state, resulting in enhanced dissolution and biological activity [36].

3.3.5. Differential scanning calorimetry

DSC is a preferred thermo-analysis to assess the molecular interactions depending on a change in the shape of thermal peak, peak temperature or enthalpy [56]. As depicted in Fig. 5, the thermogram of QCT revealed a melting endothermic peak at 167.10 °C, depicting the crystalline nature of QCT.

The thermogram of βCD exhibits two endothermic peaks at 108.84 and 320.29 °C denoting the loss of hydration water and βCD melting, respectively which is consistent with a previous report [57]. A large broad endothermic peak was observed at 89.23 °C in the thermogram of 2-HPβCD due to the loss of hydration water. No other endothermic peaks

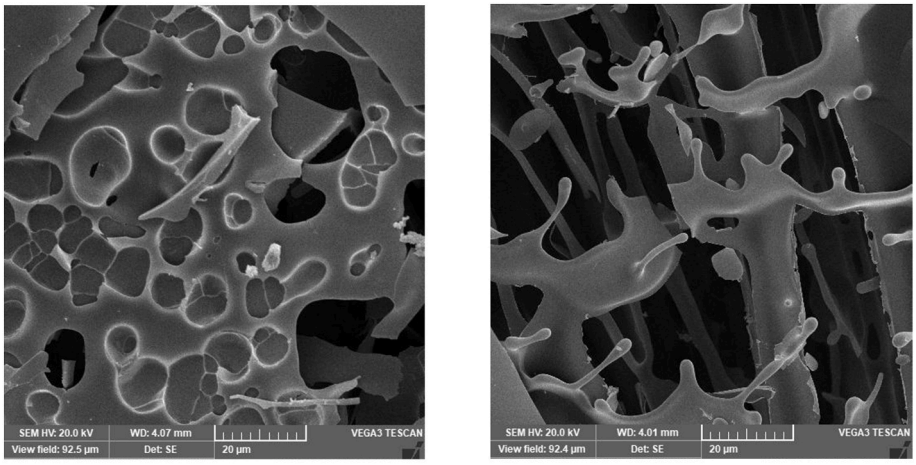

QCT-BCD/DPC 1:3 **QCT-HPBCD/DPC 1:3**

Fig. 1. SEM of QCT loaded CD-NS formulations.

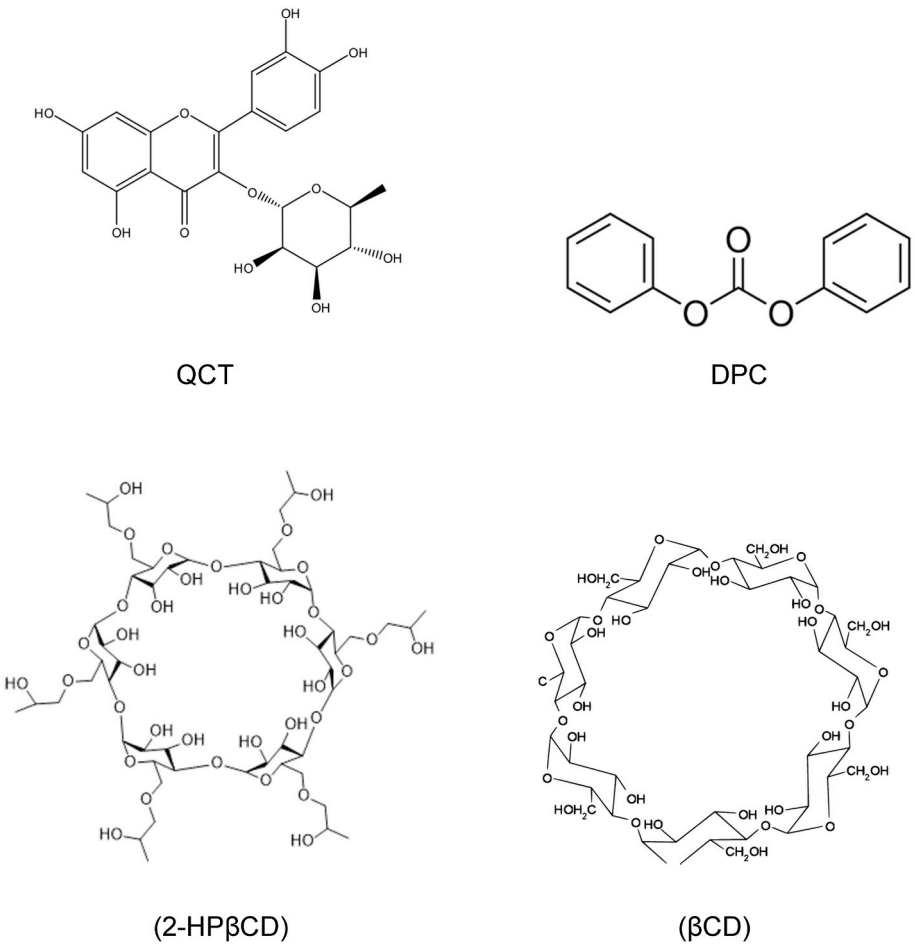

Fig. 2. Chemical structure of QCT, DPC, βCD and 2-HPβCD.

were observed as a result of amorphous nature of 2-HPβCD; this is in a good agreement with a previous report [58]. The DSC thermogram of DPC displayed an endothermic peak at 86.09 °C corresponding to its melting point which is disappeared in the DSC thermograms of plain CD-NS formulations, signifying the formation of NSs. Similarly, the melting endothermic peak of βCD (320.29 °C) disappeared in the DSC thermogram of plain BCD/DPC 1:3, indicating the formation of NS.

Regarding DSC thermograms of QCT loaded CD-NSs, it is observed that the endothermic peak of QCT is completely disappeared resulting in similarity with the plain CD-NS formulations. This indicates the inclusion of QCT in CD cavity and molecular dispersion of QCT in the crosslinked polymer matrix in an amorphous form. Similar findings were previously reported [17,26,37].Thus, DSC analysis proved the amorphous structure of the prepared CD-NSs.

3.4. *In vitro release profile of QCT from CD-NS formulations*

In vitro release of QCT from the developed formulations was carried out to investigate the impact of QCT loading into CD-NS formulations compared with free QCT.

As shown by Fig. 6, CD-NS formulations revealed enhancement of QCT release compared with the free drug suspension. The results indicated that after 24 h, 30 ± 2.52% of free QCT suspension was released which was significantly ($p < 0.05$) lower than that released from the investigated CD-NS formulations, viz., 73.82 ± 4.15 and 59.13 ± 3.25 for QCT-HPBCD/DPC 1:3 and QCT-BCD/DPC 1:3, respectively. The calculated RE $_{(0–24hr)}$ % of free QCT from its suspension was 26.88 ± 3.64% while for the investigated CD-NS formulations, RE $_{(0–24hr)}$ % were 67.68 ± 0.51 and 52.24 ± 3.52% for QCT-HPBCD/DPC 1:3 and QCT-BCD/DPC 1:3, respectively. Accordingly, RE $_{(0–24hr)}$ % of QCT was improved by 1.94–2.52 folds due to loading into CD-NS. This could be attributed to entrapment of the drug in the porous matrix of CD-NS in addition to inclusion complex with CD moiety [17,26]. Moreover, the large surface area of the nanosized CD-NS in addition to the decreased or diminished crystallinity of QCT, as revealed by XRD, could contribute to the enhanced release of QCT. In fact, crystalline form of drug is less water soluble as a result of strong attractive forces in crystals, while decreased or diminished crystallinity in CD-NS leads to enhanced drug solubility [55]. Moreover, the hydrophilic nature of CD-NS led to surface wettability with consequent increase of the drug solubility. This is consistent with previous reports regarding solubility improvement of the hydrophobic drugs loaded into CD-NS [17,39,54]. The improved release of QCT provides us with a deep insight about its improved therapeutic activity owing to its improved solubility. Fig. 6 also reveals that *in vitro* release of QCT from the investigated CD-NS formulations showed a biphasic release pattern of QCT. The initial burst release phase could be due to the presence of QCT at the surface of CD-NS; the subsequent non-burst release phase of QCT might be due to diffusion of QCT entrapped within CD-NS cavities as well as crosslinking structure of CD-NS. Similar findings have been previously reported [26,38,55].

Among QCT loaded CD-NS formulations, it is depicted that QCT-HPBCD/DPC 1:3 exhibited significant higher release efficiency ($p < 0.5$), 67.68 ± 0.51%, compared with that exhibited by QCT-BCD/DPC 1:3, 52.24 ± 3.52%. This could be explained by the fact that 2-HPβCD was reported to exhibit greater water solubility and better wetting ability compared with βCD; this results in superior enhancement in drug release [59]. Another factor is the effect of PS of CD-NS; it has been previously reported that smaller PS results in enhancement of drug

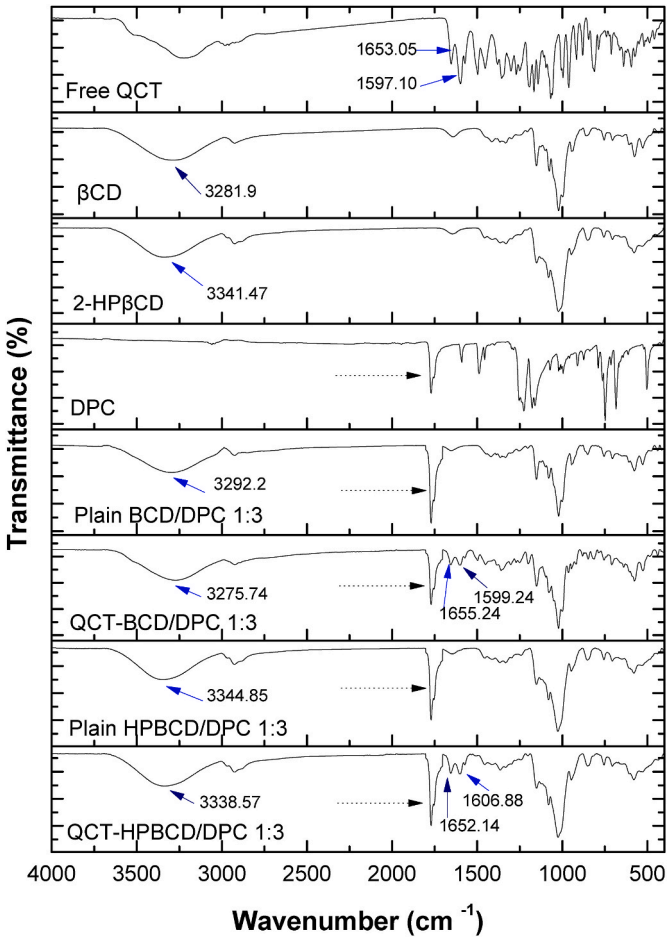

Fig. 3. FT-IR spectra of individual components, plain CD-NS and QCT loaded CD-NS formulations.

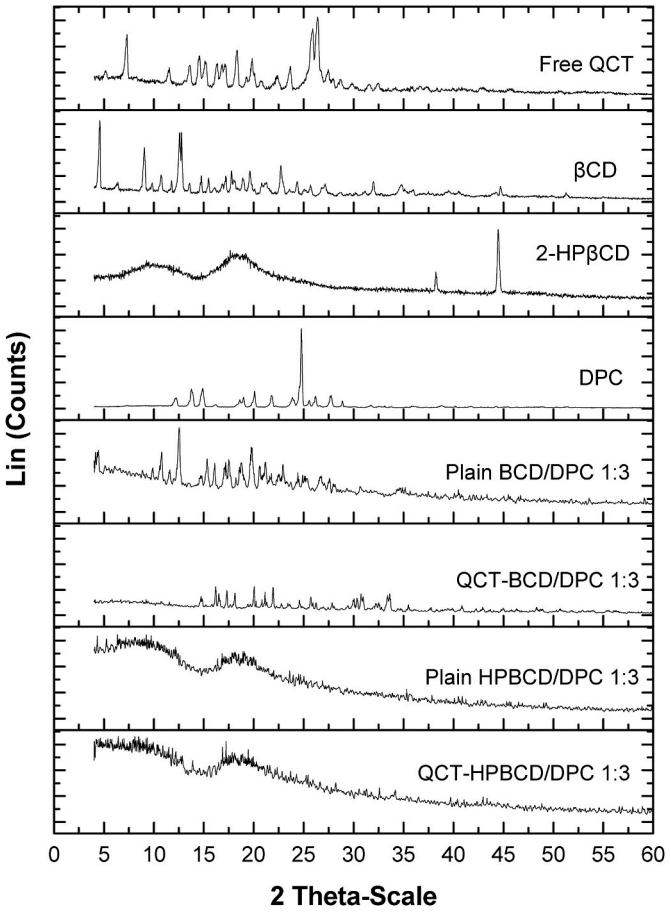

Fig. 4. XRPD diffractograms of individual components, plain CD-NS and QCT loaded CD-NS formulations.

Table (3)
FT-IR absorption frequencies of peaks of interest.

Sample	Absorption frequency (cm^{-1})		
	C=C aromatic stretching	C=O stretching	O–H stretching
QCT	1597.10	1653.05	3224.51
βCD	____	____	3281.90
2-HPβCD	____	____	3341.47
DPC	1590.73	1770.01	____
Plain BCD/DPC 1:3	____	1775.60	3292.2
QCT-BCD/DPC 1:3	1599.24	1776.43 and 1655.24	3275.74
Plain HPBCD/DPC 1:3	____	1773.80	3344.85
QCT-HPBCD/DPC 1:3	1606.88	1774.32 and 1652.14	3338.57

release due to the increased surface area of CD-NS particles [23]. QCT-HPBCD/DPC 1:3 exhibited PS (97.10 ± 8.05 nm) smaller than that of QCT-BCD/DPC 1:3 (249 ± 15.63 nm). Thus, QCT-HPBCD/DPC 1:3 revealed surface area larger than that of QCT-BCD/DPC 1:3, which probably augments the drug release. Furthermore, partial amorphization of QCT in QCT-BCD/DPC 1:3, compared with the complete drug amorphization in QCT-HPBCD/DPC 1:3, as previously discussed (section 3.3.4.), could contribute to the enhanced QCT release from QCT-HPBCD/DPC 1:3 compared with QCT-BCD/DPC 1:3.

Mathematical modeling of QCT release profile to different kinetic equations showed that Higuchi model is the most suitable model that describes QCT release from the investigated CD-NS formulations. In Higuchi model, solvent penetrates into the carrier system, dissolves drug with consequent drug release that follows Fick's law of diffusion which is dependent on square root of time. This finding is consistent with that obtained in previous reports for CD-NS systems [23,54].

3.5. *In vitro anti-proliferative activity against lung cancer cell line A549*

MTT assay, after 72 h sample incubation with cancer cell line A549, revealed anti-proliferative activity in a concentration-dependent manner for free QCT and the selected QCT loaded CD-NS formulations. In general, anti-proliferative activity exhibited by QCT on A549 lung cancer cell line was reported to be as a result of induction of apoptotic mechanism in time- and dose-dependent manner [5].

Fig. 7 demonstrates that QCT loaded CD-NS formulations achieved higher inhibition % compared with free QCT. Free QCT achieved 86% inhibition at about 450 μg/ml, while the selected QCT loaded CD-NS revealed the same inhibition (86%) at significant lower concentrations ($p < 0.05$), namely, 60.30 and 156.25 μg/ml for QCT-HPBCD/DPC 1:3 and QCT-BCD/DPC 1:3 respectively. The calculated IC_{50}, against A549 lung cells, of the selected QCT loaded CD-NS were 19.16 and 65.10 μg/ml (equivalent to QCT) for QCT-HPBCD/DPC 1:3 and QCT-BCD/DPC 1:3, respectively. On the contrary, free QCT revealed much higher IC_{50}, 102.52 μg/ml, $p < 0.05$ (Table 4). In other words, IC_{50} value of free QCT against lung cancer cell line A549 was higher than those exhibited by QCT loaded CD-NS by 5.35 and 1.57 for QCT-HPBCD/DPC 1:3 and QCT-BCD/DPC 1:3, respectively. Accordingly, anti-proliferative activity of QCT was significantly ($p < 0.05$) enhanced via loading into CD-NS. This can be attributed to particle size reduction to nanosize range

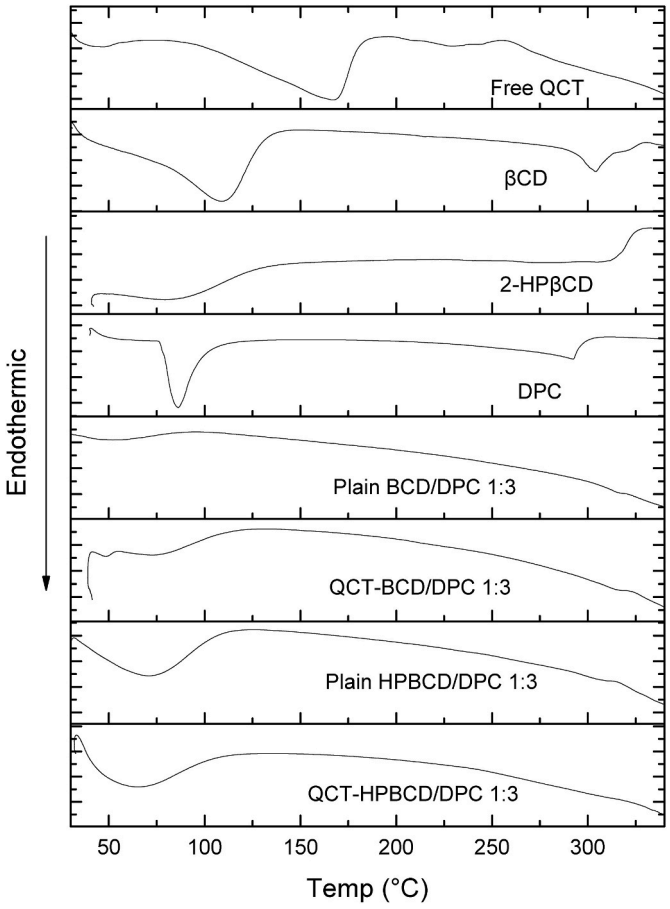

Fig. 5. DSC thermograms of individual components, plain CD-NS and QCT loaded CD-NS formulations.

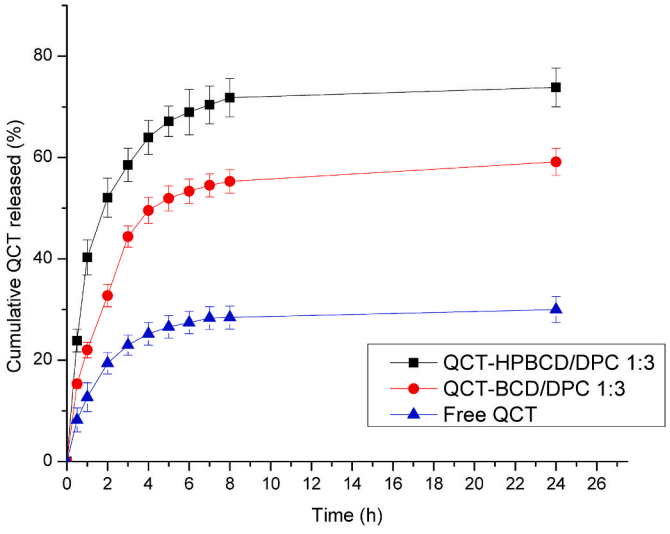

Fig. 6. *In vitro* release profiles of free QCT and the developed QCT loaded CD-NS formulations in PBS pH 7.4, at 37 °C. Each data point represents mean ± SD (n = 3).

together with enhanced release of QCT from CD-NS in a solubilized form which could result in higher cell permeability and thus higher toxicity to the cancer cells. This is consistent with the previous findings concerning loading of hydrophobic anti-cancer drugs into nanocarriers [15,17,26]. Interestingly, QCT-HPBCD/DPC 1:3 revealed IC_{50} value, 19.16 μg/ml,

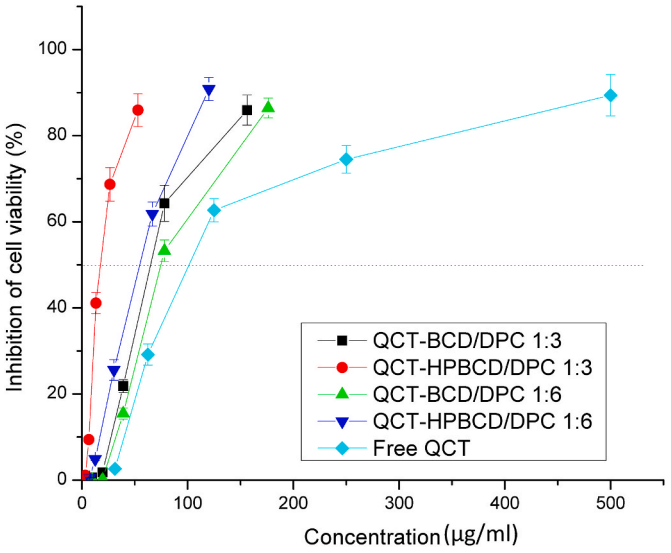

Fig. 7. Inhibition of cell viability (%) (Anti-proliferative activity %) for different concentrations, equivalent to QCT (μg/ml), for free QCT and the developed QCT loaded CD-NS formulations against lung cancer A549 cell line, as indicated by MTT assay. Each data point represents mean ± SD (n = 3).

Table (4)
IC_{50} values of QCT loaded CD-NS, the plain CD-NS formulations and free QCT for lung cancer cell line A549 (n = 3).

Code	IC_{50} (μg/mL)
Free QCT	102.52 ± 7.50
QCT-BCD/DPC 1:3	[a] 65.10 ± 4.10
QCT-BCD/DPC 1:6	[a] 73.33 ± 5.24
QCT-HPBCD/DPC 1:3	[a] 19.16 ± 0.86
QCT-HPBCD/DPC 1:6	[a] 53.83 ± 3.8
Plain BCD/DPC 1:3	450.25 ± 30.21
Plain HPBCD/DPC 1:3	463.00 ± 25.19
Plain BCD/DPC 1:6	421.40 ± 25.21
Plain HPBCD/DPC 1:6	445.87 ± 32.65

[a] Equivalent to QCT.

lower than that revealed by QCT-BCD/DPC 1:3, 65.10 μg/ml. This could be explained by several factors: First, the smaller PS of QCT-HPBCD/DPC 1:3 compared with that of QCT-BCD/DPC 1:3 (Table 2). This hypothesis is confirmed by the higher IC_{50} values of their counterparts employing CD:DPC molar ratio 1:6 (Table 4). Thus, PS has a direct relation with IC_{50}. Second, QCT-HPBCD/DPC 1:3 revealed a significant ($p < 0.05$) higher release efficiency, 67.68 ± 0.51%, compared with that of QCT-BCD/DPC 1:3, 52.24 ± 3.52% which is related to partial amorphization of QCT in QCT-BCD/DPC 1:3, compared with the complete drug amorphization in QCT-HPBCD/DPC 1:3, as previously discussed (section 3.3.4.). The above mentioned two reasons provide additional confirmation of the crucial role of PS and drug release from CD-NS, in a solubilized form, for anti-proliferative activity of the loaded hydrophobic drug.

3.5.1. Anti-proliferative activity of plain CD-NS formulations against lung cancer cell line A549

Fig. 8 reveals the percentage of viable A549 lung cells incubated with plain CD-NS for 72 h. Plain CD-NS had no significant ($p > 0.5$) effect on the viability of A549 lung cells at concentrations ranging from 31.25 to 125 μg/ml. At a higher concentration (250 μg/ml), cell viability was decreased. The decrease of cell viability revealed by plain CD-NS could be explained by the finding of a previous report where CD itself exhibited anti-proliferative activity by reducing intracellular cholesterol leading to significant leukemic cell growth inhibition [60]. Concerning

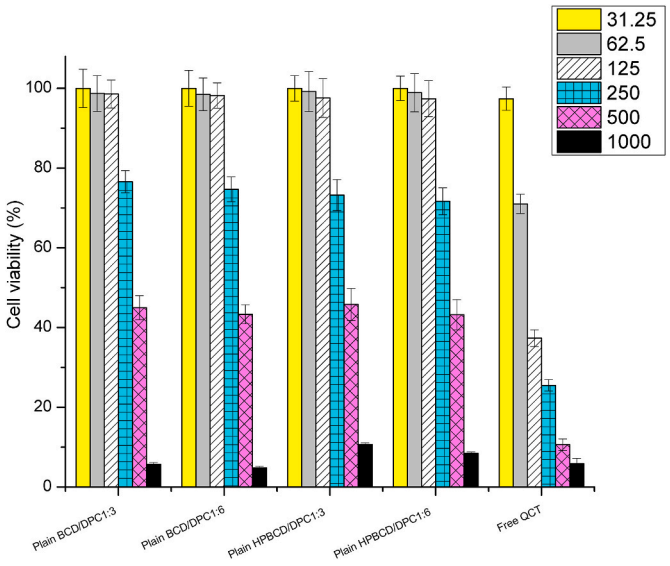

Fig. 8. Cell viability (%) for different concentrations (μg/ml) of free QCT and plain CD-NS formulations against lung cancer A549 cell line, as indicated by MTT assay. Each data point represents mean ± SD (n = 3).

free QCT, it exhibited no effect on cell viability only at very dilute concentration, 31.25 μg/ml. A substantial decrease in cell viability was observed upon increasing concentrations of free QCT. Free QCT at concentration of 500 μg/ml exhibited significant ($p < 0.05$) lower cell viability, 10.60%, compared with 43.21–45.80 for plain CD-NS at the same concentration. This finding proves that the plain CD-NSs have a weaker effect on A549 lung cell viability as they exhibited significant ($p < 0.05$) higher IC_{50} values compared with IC_{50} of free QCT (Table 4). Accordingly, the improved anti-proliferative activity of the investigated QCT loaded CD-NSs is due to the positive impacts of QCT loading into CD-NSs, as described in the previous section (section 3.5).

The cell viabilities of A549 lung cancer cells treated with very high concentration (1000 μg/ml) of the investigated plain CD-NS formulations as well as free QCT are almost the same, ranged between 5.90 and 10.70%. However, this concentration is much higher than that required to achieve IC_{50} for QCT either free or loaded in CD-NS formulations.

3.6. Anti-SARS-CoV-2 activity and cytotoxicity against normal Vero-E6 cells

Anti-SARS-CoV-2 activity and cytotoxicity of QCT loaded CD-NS, plain CD-NS formulations as well as free QCT were assessed. Regarding anti-SARS-CoV-2 activity, Fig. 9 shows that free QCT exhibited IC_{50}, 438.40 μg/ml. This is higher than those exhibited by QCT-HPBCD/DPC 1:3 and QCT-BCD/DPC 1:3 by 26.95 and 5.95 folds, respectively. This finding signifies the superior activity of QCT loaded CD-NSs over free QCT. This could be ascribed to the nanosized particles of the prepared QCT loaded CD-NS formulations together with enhanced release of QCT from CD-NSs in a solubilized form which could result in higher anti-viral toxicity [61]. Interestingly, QCT-HPBCD/DPC 1:3 revealed IC_{50}, 16.27 μg/ml; this is lower than that revealed by QCT-BCD/DPC 1:3, 73.73 μg/ml. This may be attributed to the crucial role of PS and drug release from CD-NSs, in a solubilized form, for enhancing the biological activity of the loaded hydrophobic drug, as previously discussed (section 3.5.).

Concerning plain CD-NS formulations, they showed significant ($p < 0.05$) higher IC_{50} values compared with those exhibited by QC loaded CD-NS formulations indicating weak anti-viral effect of plain CD-NSs.

Regarding cytotoxicity, Fig. 9 reveals that CC_{50} values of the developed CD-NSs, either plain or loaded with QCT, as well as free QCT against normal Vero-E6 cells are much higher than their IC_{50} values against SARS-CoV-2, indicating their safety. Calculated SI for QCT-HPBCD/DPC 1:3 and QCT-BCD/DPC 1:3 were 17.73 and 29.40, respectively which are significantly ($p < 0.05$) higher than SI of free QCT (3.98). This indicates a higher selectivity of QCT loaded CD-NS, and thus safety, compared with free QCT.

In summary, the positive impacts of PS of the developed CD-NS formulations on the enhancement of QCT solubility and consequently its biological activity have been proved. The two types of QCT loaded CD-NS formulations, QCT-HPBCD/DPC 1:3 and QCT-BCD/DPC 1:3, depicted PS in the nanorange. The lower PS of QCT-HPBCD/DPC 1:3 (97.10 nm) compared with that of QCT-BCD/DPC 1:3 (249 nm) could explain the superiority of the former compared with that of the later regarding *in vitro* release profile, anti-proliferative and anti-SARS-CoV-2 activity of the entrapped QCT. The two types of the developed QCT loaded CD-NS formulations revealed an obvious superiority over the free QCT regarding the investigated biological activities.

4. Conclusion

In the current study, two types of CD-NS formulations were developed for loading of QCT in an attempt to enhance the aqueous solubility of QCT for augmenting its biological activities, namely, anti-proliferative and anti-SARS-CoV-2 activities. The developed QCT loaded CD-NS revealed high EE% of QCT (94.17–99.31%) with PS in the nanosize range. FT-IR spectroscopy proved the formation of QCT loaded CD-NSs. XRPD depicted partial amorphization of QCT in QCT-BCD/DPC 1:3, compared with the complete drug amorphization in QCT-HPBCD/DPC 1:3. QCT loaded CD-NS formulations exhibited sponge-like morphology, as shown by SEM. *In vitro* release study revealed the enhancement of QCT release from the developed formulations indicating its improved solubilization. IC_{50} of free QCT against lung cancer cell line A549 was higher than those exhibited by the developed QCT loaded CD-NS formulations by 1.57–5.35 folds. Concerning SARS-CoV-2 activity, free QCT exhibited IC_{50} value higher than those of the developed QCT loaded CD-NS formulations by 5.95–26.95 folds. Interestingly, QCT loaded CD-NS employing 2-HPβCD (QCT-HPBCD/DPC 1:3) exhibited superiority over QCT loaded CD-NS employing βCD (QCT-BCD/DPC 1:3) concerning *in vitro* release profile, anti-proliferative and anti-SARS-CoV-2 activity of the entrapped QCT. This could be explained by the greater water solubility and better wetting ability of 2-HPβCD compared with βCD.

The results of the current study signified the potential of incorporating QCT in the nanosized CD-NS as an effective means to improve its aqueous solubility and consequently, its biological activity against lung cancer and SARS-CoV-2. The obtained findings could be considered as a base for further study on animals through administration by parenteral or oral route.

CRediT author statement

Sally Abou Taleb: Conceptualization, Methodology, Resources. **Yassmin Moatasim:** Conceptualization, Methodology, Formal analysis, Resources, Writing- Original draft. **Mohamed GabAllah:** Conceptualization, Methodology, Resources. **Marwa Hasanein Asfour:** Conceptualization, Methodology, Formal analysis, Writing- Original draft, visualization, Validation.

Declaration of competing interest

The authors declare that they have no known competing financial interests or personal relationships that could have appeared to influence the work reported in this paper. Marwa Asfour reports financial support was provided by National Research Centre, Egypt.

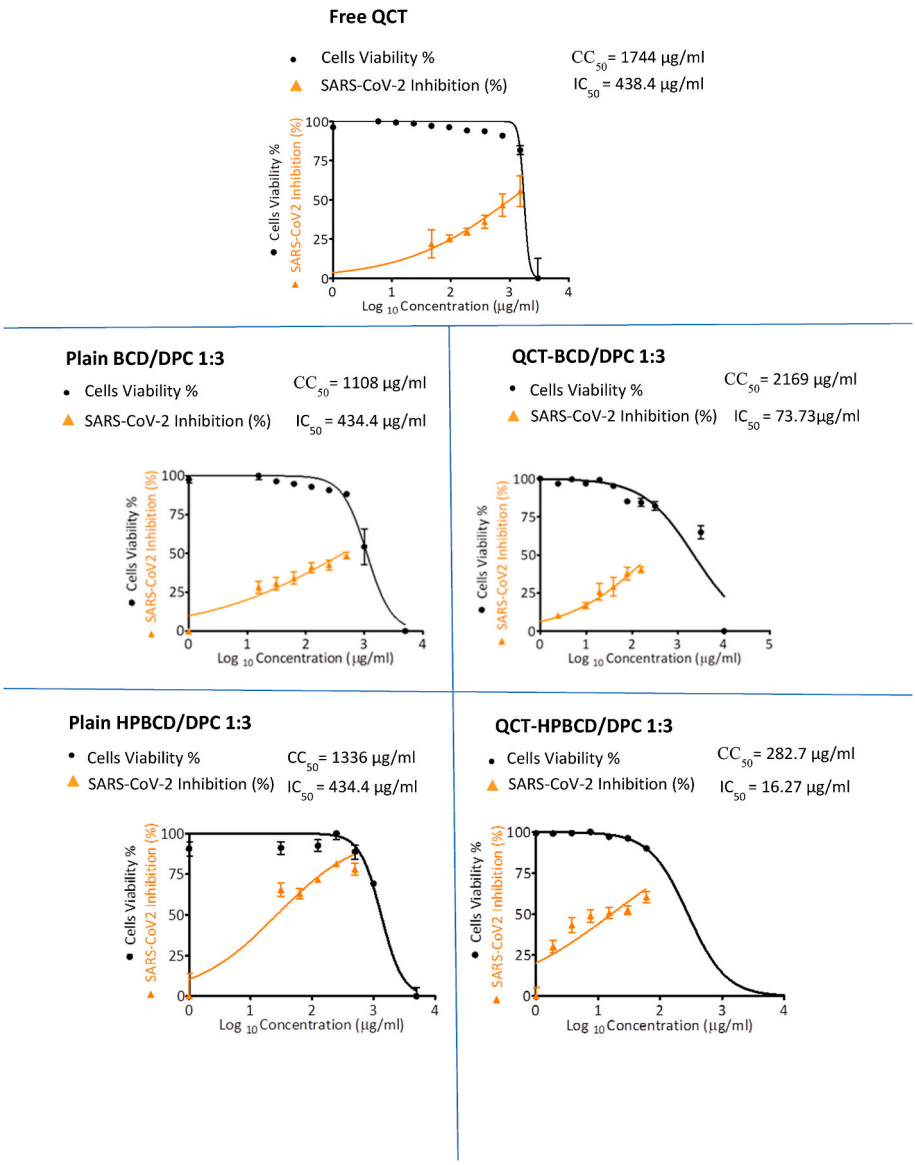

Fig. 9. *Anti*-SARS-CoV-2 activity and cytotoxicity against normal Vero-E6 cells for free QCT, plain CD-NS and QCT loaded CD-NS formulations. Each data point represents mean ± SD (n = 3).

Data availability

Data will be made available on request.

Acknowledgements

This work was supported by the National Research Centre, Cairo, Egypt.

References

[1] H. Sung, et al., Global cancer statistics 2020: GLOBOCAN estimates of incidence and mortality worldwide for 36 cancers in 185 countries, CA A Cancer J. Clin. 71 (3) (2021) 209–249.
[2] K. Islam, et al., Patient preferences of chemotherapy treatment options and tolerance of chemotherapy side effects in advanced stage lung cancer, BMC Cancer 19 (1) (2019) 1–9.
[3] E.S. Kim, Chemotherapy resistance in lung cancer, Adv. Exp. Med. Biol. 893 (2016) 189–209.
[4] S. Mateen, K. Raina, R. Agarwal, Chemopreventive and anti-cancer efficacy of silibinin against growth and progression of lung cancer, Nutr. Cancer 65 (Suppl 1) (2013) 3–11.
[5] Z.B. Cincin, et al., Molecular mechanisms of quercitrin-induced apoptosis in non-small cell lung cancer, Arch. Med. Res. 45 (6) (2014) 445–454.
[6] P. Zhou, et al., A pneumonia outbreak associated with a new coronavirus of probable bat origin, Nature 579 (7798) (2020) 270–273.
[7] B. Hu, et al., Characteristics of SARS-CoV-2 and COVID-19, Nat. Rev. Microbiol. 19 (3) (2021) 141–154.
[8] R.M.L. Colunga Biancatelli, et al., Quercetin and vitamin C: an experimental, synergistic therapy for the prevention and treatment of SARS-CoV-2 related disease (COVID-19), Front. Immunol. 11 (2020) 1451.
[9] O. Benavente-Garcia, J. Castillo, Update on uses and properties of citrus flavonoids: new findings in anticancer, cardiovascular, and anti-inflammatory activity, J. Agric. Food Chem. 56 (15) (2008) 6185–6205.
[10] A.N. Panche, A.D. Diwan, S.R. Chandra, Flavonoids: an overview, J. Nutr. Sci. 5 (2016) e47.
[11] M.S. Hasan, et al., Antioxidant, antinociceptive activity and general toxicity study of Dendrophthoe falcata and isolation of quercitrin as the major component, Orient. Pharm. Exp. Med. 6 (4) (2006) 355–360.
[12] R. Hardiyanti, et al., Isolation of quercitrin from dendrophthoe pentandra (L.) Miq leaves and its antioxidant and antibacterial activities, Rasayan J. Chem. 12 (3) (2019) 1822–1827.
[13] H.J. Choi, et al., Inhibitory effects of quercetin 3-rhamnoside on influenza A virus replication, Eur. J. Pharmaceut. Sci. 37 (3–4) (2009) 329–333.
[14] M. Saakre, D. Mathew, V. Ravisankar, Perspectives on plant flavonoid quercetin-based drugs for novel SARS-CoV-2, Beni-Suef Univ. J. Basic. Appl. Sci. 10 (2021) 1–13.

[15] M.H. Asfour, A.M. Mohsen, Formulation and evaluation of pH-sensitive rutin nanospheres against colon carcinoma using HCT-116 cell line, J. Adv. Res. 9 (2018) 17–26.
[16] M.H. Asfour, A.A.A. Salama, A.M. Mohsen, Fabrication of all-trans retinoic acid loaded chitosan/tripolyphosphate lipid hybrid nanoparticles as a novel oral delivery approach for management of diabetic nephropathy in rats, J. Pharmacol. Sci. 110 (9) (2021) 3208–3220.
[17] R. Pushpalatha, S. Selvamuthukumar, D. Kilimozhi, Cross-linked, cyclodextrin-based nanosponges for curcumin delivery-Physicochemical characterization, drug release, stability and cytotoxicity, J. Drug Deliv. Sci. Technol. 45 (2018) 45–53.
[18] A.C. Santos, et al., Cyclodextrin-based delivery systems for in vivo-tested anticancer therapies, Drug Deliv. Transl. Res. 11 (1) (2021) 49–71.
[19] S. Jacob, A.B. Nair, Cyclodextrin complexes: perspective from drug delivery and formulation, Drug Dev. Res. 79 (5) (2018) 201–217.
[20] V. Venuti, et al., Tuning structural parameters for the optimization of drug delivery performance of cyclodextrin-based nanosponges, Expert Opin. Drug Deliv. 14 (3) (2017) 331–340.
[21] G. Utzeri, et al., Cyclodextrin-based nanosponges: overview and opportunities, Front. Chem. 10 (2022).
[22] R.Z. Ahmed, G. Patil, Z. Zaheer, Nanosponges - a completely new nano-horizon: pharmaceutical applications and recent advances, Drug Dev. Ind. Pharm. 39 (9) (2013) 1263–1272.
[23] G. Yaşayan, et al., Fabrication and characterisation studies of cyclodextrin-based nanosponges for sulfamethoxazole delivery, J. Inclusion Phenom. Macrocycl. Chem. 97 (2020) 175–186.
[24] S. Swaminathan, et al., Cyclodextrin-based nanosponges encapsulating camptothecin: physicochemical characterization, stability and cytotoxicity, Eur. J. Pharm. Biopharm. 74 (2) (2010) 193–201.
[25] S. Swaminathan, et al., Structural evidence of differential forms of nanosponges of beta-cyclodextrin and its effect on solubilization of a model drug, J. Inclusion Phenom. Macrocycl. Chem. 76 (1) (2013) 201–211.
[26] A. Rezaei, et al., Improving the solubility and in vitro cytotoxicity (anticancer activity) of ferulic acid by loading it into cyclodextrin nanosponges, Int. J. Nanomed. 14 (2019) 4589–4599.
[27] M. Argenziano, et al., Improvement in the anti-tumor efficacy of doxorubicin nanosponges in in vitro and in mice bearing breast tumor models, Cancers 12 (1) (2020).
[28] B. Mognetti, et al., In vitro enhancement of anticancer activity of paclitaxel by a Cremophor free cyclodextrin-based nanosponge formulation, J. Inclusion Phenom. Macrocycl. Chem. 74 (1–4) (2012) 201–210.
[29] S.M. Shawky, M.K. Khalifa, H.A. Eassa, Lornoxicam-loaded nanosponges for controlled anti-inflammatory effect: in vitro/in vivo assessment, Int. J. Appl. Pharm. 12 (6) (2020) 217–223.
[30] D. Lembo, et al., Encapsulation of acyclovir in new carboxylated cyclodextrin-based nanosponges improves the agent's antiviral efficacy, Int. J. Pharm. 443 (1–2) (2013) 262–272.
[31] R. Zainuddin, et al., Enhancement of oral bioavailability of anti-HIV drug rilpivirine HCl through nanosponge formulation, Drug Dev. Ind. Pharm. 43 (12) (2017) 2076–2084.
[32] I. García-Silva, G. Palestino, O. Gonzalez-Ortega, Chapter 17 - the potential of drug delivery nanosystems to treat COVID-19, in: M. Comas-Garcia, O. Gonzalez-Ortega (Eds.), *Biomedical Innovations To Combat COVID-19*, S. Rosales-Mendoza, Academic Press, 2022, pp. 307–337.
[33] S.M. Aljubiri, et al., Bioactive compounds from Euphorbia schimperiana with cytotoxic and antibacterial activities, South Afr. J. Bot. 141 (2021) 357–366.
[34] A. Kandeil, et al., Coding-complete genome sequences of two SARS-CoV-2 isolates from Egypt, Microbiol. Resour. Announc. 9 (22) (2020) e00489–20.
[35] S. Abou Taleb, et al., Investigation of a new horizon antifungal activity with enhancing the antimicrobial efficacy of ciprofloxacin and its binary mixture via their encapsulation in nanoassemblies: in vitro and in vivo evaluation, Drug Dev. Res. 81 (3) (2020) 374–388.
[36] S. Kumar, M. Prasad, R. Rao, Topical delivery of clobetasol propionate loaded nanosponge hydrogel for effective treatment of psoriasis: formulation, physicochemical characterization, antipsoriatic potential and biochemical estimation, Mater. Sci. Eng. C Mater Biol. Appl. 119 (2021), 111605.
[37] S.M. Omar, F. Ibrahim, A. Ismail, Formulation and evaluation of cyclodextrin-based nanosponges of griseofulvin as pediatric oral liquid dosage form for enhancing bioavailability and masking bitter taste, Saudi Pharmaceut. J. 28 (3) (2020) 349–361.
[38] S. Darandale, P. Vavia, Cyclodextrin-based nanosponges of curcumin: formulation and physicochemical characterization, J. Inclusion Phenom. Macrocycl. Chem. 75 (3–4) (2013) 315–322.
[39] K.A. Ansari, et al., Cyclodextrin-based nanosponges for delivery of resveratrol: in vitro characterisation, stability, cytotoxicity and permeation study, AAPS PharmSciTech 12 (1) (2011) 279–286.
[40] A.M. Mohsen, M.H. Asfour, A.A.A. Salama, Improved hepatoprotective activity of silymarin via encapsulation in the novel vesicular nanosystem bilosomes, Drug Dev. Ind. Pharm. 43 (12) (2017) 2043–2054.
[41] K.A. Khan, The concept of dissolution efficiency, J. Pharm. Pharmacol. 27 (1) (1975) 48–49.
[42] S. Dash, et al., Kinetic modeling on drug release from controlled drug delivery systems, Acta Pol. Pharm. 67 (3) (2010) 217–223.
[43] A.A. van de Loosdrecht, et al., A tetrazolium-based colorimetric MTT assay to quantitate human monocyte mediated cytotoxicity against leukemic cells from cell lines and patients with acute myeloid leukemia, J. Immunol. Methods 174 (1–2) (1994) 311–320.
[44] M. Ashjaran, et al., Stimuli-responsive polyvinylpyrrolidone-NIPPAm-lysine graphene oxide nano-hybrid as an anticancer drug delivery on MCF7 cell line, Artif. Cell Nanomed. Biotechnol. 47 (1) (2019) 443–454.
[45] A. Mostafa, et al., FDA-approved drugs with potent in vitro antiviral activity against severe acute respiratory syndrome coronavirus 2, Pharmaceuticals 13 (12) (2020).
[46] M. Feoktistova, P. Geserick, M. Leverkus, Crystal violet assay for determining viability of cultured cells, 2016, Cold Spring Harb. Protoc. (4) (2016). pdb. prot087379.
[47] I.A. Seliem, et al., New quinoline-triazole conjugates: synthesis, and antiviral properties against SARS-CoV-2, Bioorg. Chem. 114 (2021), 105117.
[48] F. Trotta, M. Zanetti, R. Cavalli, Cyclodextrin-based nanosponges as drug carriers, Beilstein J. Org. Chem. 8 (1) (2012) 2091–2099.
[49] P. Iriventi, et al., Design & development of nanosponge loaded topical gel of curcumin and caffeine mixture for augmented treatment of psoriasis, Daru 28 (2) (2020) 489–506.
[50] D.M. Mostafa, et al., Transdermal fennel essential oil nanoemulsions with promising hepatic dysfunction healing effect: in vitro and in vivo study, Pharmaceut. Dev. Technol. 24 (6) (2019) 729–738.
[51] M.F. Zidan, et al., In vitro and in vivo evaluation of cyclodextrin-based nanosponges for enhancing oral bioavailability of atorvastatin calcium, Drug Dev. Ind. Pharm. 44 (8) (2018) 1243–1253.
[52] Q.U. Shoaib, et al., Solubility and dissolution rate enhancement of ibuprofen by cyclodextrin based carbonate nanosponges, Supplementary, Pak. J. Pharm. Sci. 34 (3) (2021) 1045–1055.
[53] N.N.S. Mai, et al., Enhancing the solubility of curcumin using a solid dispersion system with hydroxypropyl-β-cyclodextrin prepared by grinding, freeze-drying, and common solvent evaporation methods, Pharmacy 8 (4) (2020) 203.
[54] S.G. Patel, S.J. Rajput, Enhancement of oral bioavailability of cilostazol by forming its inclusion complexes, AAPS PharmSciTech 10 (2) (2009) 660–669.
[55] Q. Khalid, et al., Novel β-cyclodextrin nanosponges by chain growth condensation for solubility enhancement of dexibuprofen: characterization and acute oral toxicity studies, J. Drug Deliv. Sci. Technol. 61 (2021), 102089.
[56] A.A. Kassem, et al., Phospholipid complex enriched micelles: a novel drug delivery approach for promoting the antidiabetic effect of repaglinide, Eur. J. Pharmaceut. Sci. 99 (2017) 75–84.
[57] A. Farcas, et al., Synthesis and characterization of furosemide complex in β-cyclodextrin, Dig J. Nanomater Biostruct. 1 (2) (2006) 55–60.
[58] H. Cui, S. Siva, L. Lin, Ultrasound processed cuminaldehyde/2-hydroxypropyl-beta-cyclodextrin inclusion complex: preparation, characterization and antibacterial activity, Ultrason. Sonochem. 56 (2019) 84–93.
[59] N. Elgindy, et al., Lyophilization monophase solution technique for improvement of the physicochemical properties of an anticancer drug, flutamide, Eur. J. Pharm. Biopharm. 74 (2) (2010) 397–405.
[60] M. Yokoo, et al., 2-Hydroxypropyl-beta-Cyclodextrin acts as a novel anticancer agent, PLoS One 10 (11) (2015), e0141946.
[61] R. Chen, et al., Antiviral drug delivery system for enhanced bioactivity, better metabolism and pharmacokinetic characteristics, Int. J. Nanomed. 16 (2021) 4959–4984.